ELSEVIER

S0032-3861(96)00376-X

Polymer Vol. 37 No. 21, pp. 4857–4863, 1996

0032-3861/96/$15.00 + 0.00

Effects of annealing on the disappearance and creation of constrained amorphous phase

Sharon Xin Lu* and Peggy Cebe†
Department of Materials Science and Engineering, Massachusetts Institute of Technology, Cambridge, MA 02139, USA
(Received 21 July 1995; revised 19 February 1996)

We report observation of the disappearance and recreation of the rigid, or constrained, amorphous phase by sequential thermal annealing. Modulated differential scanning calorimetry (m.d.s.c.) is used to study the glass transition and lower melting endotherm after annealing. Cold crystallization at a temperature T_{cc} just above T_g creates an initial large fraction of rigid amorphous phase (RAP). Brief rapid annealing to a higher temperature causes the constrained amorphous phase almost to disappear completely, a result that has never been reported before. Subsequent reannealing at the original lower temperature T_{cc} restores RAP to its original value. At the same time that RAP is being removed, the glass transition temperature decreases; when RAP is restored, T_g increases once again. The crystal fraction remains unaffected by the annealing sequence. Results indicate that the location of the RAP is within the amorphous phase, rather than in a separate location away from the liquid-like amorphous phase. Copyright © 1996 Elsevier Science Ltd.

(Keywords: modulated differential scanning calorimetry; rigid amorphous phase; glass transition)

Introduction

Failure of the two-phase model to describe morphology in semicrystalline polymers has been a subject of study from the early 1960s[1–8]. Recent studies in this area have been concerned with the nature of the amorphous phase and its relationship to the crystals in high performance semicrystalline polymers, like poly(etheretherketone), PEEK[9–12], poly(phenylene sulfide), PPS[13–16], and poly(ethylene terephthalate), PET[17,18]. The mechanical properties of these materials are strongly reinforced by the crystal phase, even though degree of crystallinity is usually modest at about 0.40 or less. The amorphous phase serves to transfer stresses to the crystals across the crystal/amorphous interphase. Thus, the properties of the amorphous phase glass transition relaxation, and the reinforcing effect of the crystals, are important for the ultimate use of these polymers.

Recent studies have indicated that the amorphous phase in these high performance polymers is complex. Not all of the amorphous phase relaxes at the nominal T_g during thermal analysis by differential scanning calorimetry (d.s.c.)[6–11]. The 'rigid amorphous phase', or RAP, is that portion of the amorphous phase which does not undergo a distinct glass transition relaxation[6–11]. Only the most mobile, or liquid-like amorphous phase, undergoes the glass transition relaxation process during normal d.s.c. testing. Several general observations can be made concerning the amount and behaviour of constrained amorphous phase. First, RAP content is greatest under crystallization conditions that favour formation of imperfect crystals. These include rapid non-isothermal cooling from the melt, and crystallization of quenched polymer by heating about T_g ('cold' crystallization at T_{cc}). Second, at the end of isothermal cold crystallization the amount of crystals is larger, and the amount of constrained amorphous phase is smaller, when the cold crystallization temperature, T_{cc}, is increased.

Cold crystallization of quenched polymer nearly always results in a lower melting endotherm which occurs 10–15°C above T_{cc}, in addition to the higher melting endotherm whose position does not change much with T_{cc}. Multiple melting endotherms have been observed in many polymers including PEEK[11,19–27], PET[28,29], PBT[30,31] and PPS[13–16,32,33]. The lower melting endotherm shifts to higher temperature as T_{cc} increases. Since cold crystallization also results in formation of a large fraction of RAP, and RAP content decreases as T_{cc} increases, we suggest that there may be an association between the creation of constrained amorphous phase and the creation of the lower melting endotherm. To examine the nature of the constrained amorphous phase we have used the new technique of modulated differential scanning calorimetry (m.d.s.c.) to study the glass transition relaxation and the lower melting endotherm after a sequential annealing process.

M.d.s.c. has brought a new dimension to thermal analysis[34–38]. Excellent review of this technique can be found in ref. 34. M.d.s.c. is able to separate the total heat flow into two parts: (1) the heat flow from the heat capacity effect that usually comes from glass transition relaxation or crystal melting; and (2) the heat flow from the non-heat capacity effect that usually comes from

* Present address: Exxon Chemical Corp., 5200 Bayway Drive, Baytown, TX 77522, USA
† Present address: Tufts University, Department of Physics and Astronomy, Science & Technology Center, Room 208, 4 Colby Street, Medford, MA 02155, USA. To whom correspondence should be addressed

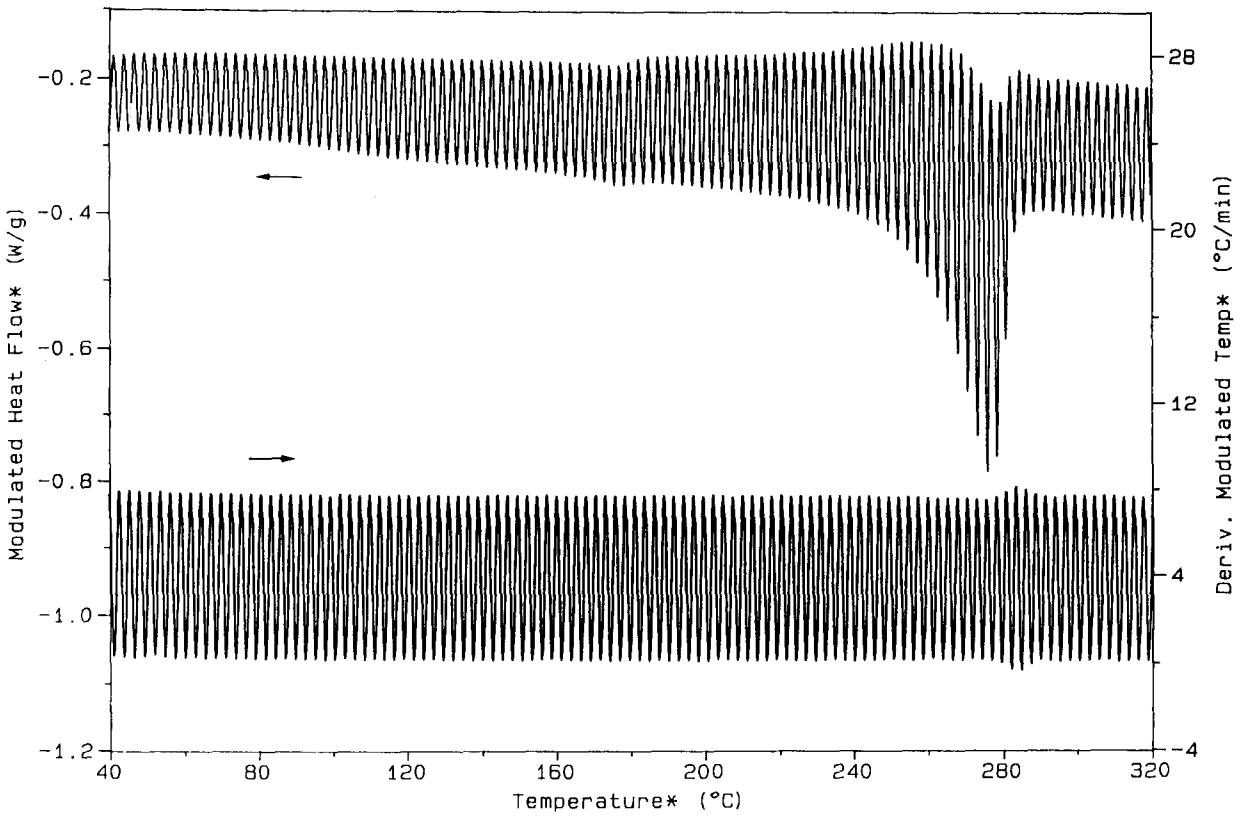

Figure 1 M.d.s.c. raw data from the Type A sample. The upper curve represents the modulated heat flow, the lower curve represents the actual heating rate

enthalpic relaxation or cold crystallization. In this work, we will show directly from m.d.s.c. that the origin of the lower temperature peak is due primarily to crystal melting and to a much lesser extent, enthalpic relaxation. Cold crystallization occurs immediately after the sample is heated above its previous treatment temperature. Using sequential annealing we show that RAP can be *removed* by brief exposure to elevated temperature, and *recreated* by annealing at a lower temperature. At the same time that RAP is removed, the glass transition temperature of the liquid-like amorphous phase decreases; when RAP is subsequently restored, T_g increases again. The annealing leaves the crystal fraction unaltered, but does affect the appearance of the lower melting endotherm.

Experimental

The material used in this study is PPS, Ryton V-1 grade from Phillips Petroleum Company. This polymer was chosen because it displays a very large amount of RAP when it is cold crystallized[13,14]. The as-received material was a semicrystalline sheet with a thickness of 75 μm and molecular weight of 60 000 g mol^{-1}. The amorphous samples were prepared by first melting the sample at 320°C for 2 min to destroy the crystal seeds, then quickly quenching into ice water. The amorphous samples were encapsulated in d.s.c. pans and treated inside a differential scanning calorimeter (Perkin Elmer DSC-4) under different annealing conditions. Type A samples were prepared by heating from 60 to 170°C at a heating rate of 20°C min^{-1}, holding at T_{cc} = 170°C for 30 min, then cooling to 40°C at a nominal cooling rate of 200°C min^{-1}. Type B samples were prepared as Type A samples, but after the annealing step at 170°C, the samples were heated momentarily to 210°C at 20°C min^{-1}, then immediately cooled to 40°C at 200°C min^{-1}. Type C samples were first treated as Type B samples, then were reheated to 170°C and held for 30 min, and finally cooled to 40°C at 200°C min^{-1}.

Thermal analysis was subsequently performed using a Modulated DSC from TA instruments. Both temperature and baseline were calibrated as in conventional d.s.c. High density polyethylene was used to calibrate heat capacity. A scan rate of 4°C min^{-1} was used with a temperature modulation amplitude of 0.42°C and a temperature modulation period of 40 s. These modulation parameters were chosen so that the heating rate was always above zero, i.e., no cooling occurred during the scanning process[35] for the temperature region of interest, below 270°C. In order to maximize the signal as well as to reduce the heat transfer delay, an average sample weight of 10 mg was used. The weight of the sample pan and reference pan are carefully matched. Helium was used as a heat transfer gas at a flow rate of 30 ml min^{-1}.

Exactly similar studies were carried out using a Perkin Elmer DSC-4 operated at 20°C min^{-1} heating rate. In this report, these results are not shown for the sake of brevity. In all cases, the d.s.c. scans showed the same features and relative peak heights as the m.d.s.c. total heat flow curves. The only differences were due to the different heating rates used in the two instruments.

Results

In *Figure 1*, we present the m.d.s.c. raw data obtained from the Type A sample. The upper curve gives the modulated heat flow, while the lower curve shows the

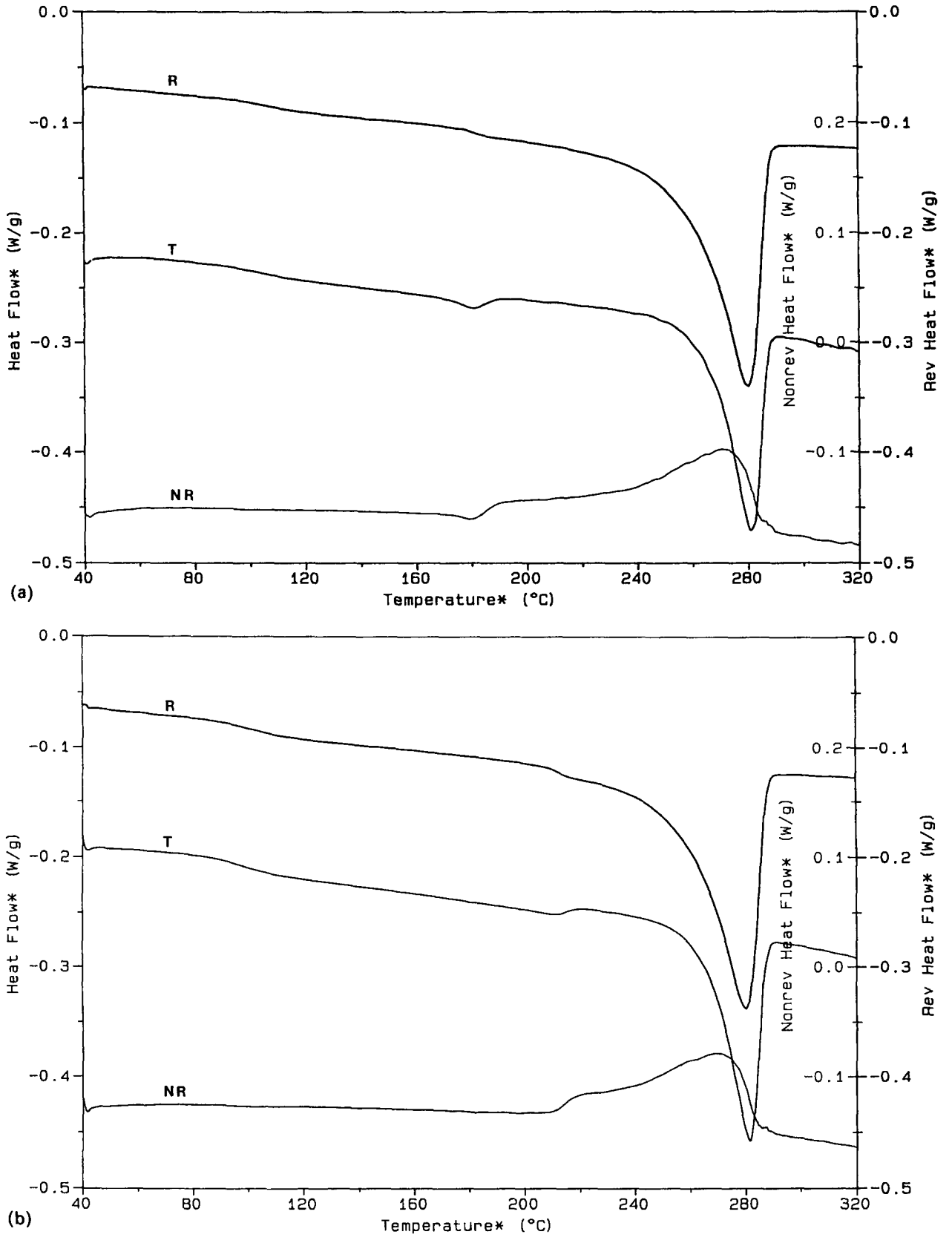

Figure 2 Total heat flow, reversing heat flow and non-reversing heat flow obtained from m.d.s.c. for three types of samples: (a) Type A, (b) Type B, and (c) Type C

simultaneous heating rate. Almost at all times, the heating rate is above zero, i.e. the sample does not experience cooling. The slightly negative heating rate at the higher temperature end is the result of previous large crystal melting. As we have discussed earlier, three heat flow curves can be derived from these raw data. The results are shown in *Figures 2a, b* and *c* for Type A, B, and C samples, respectively. Each plot consists of three

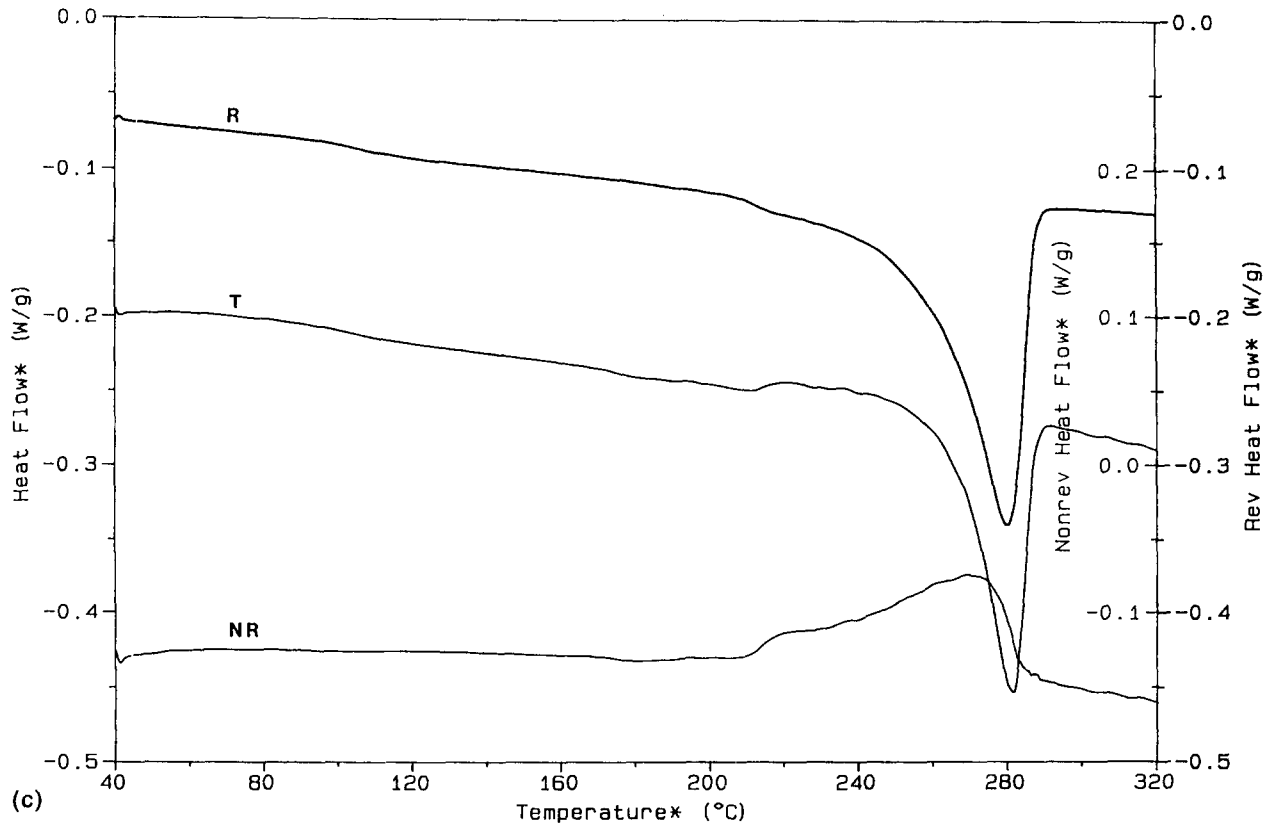

Figure 2 (*Continued*)

Table 1 Thermal properties of PPS samples: glass transition temperature, heat of fusion from total, reversing and non-reversing heat flow, and mass fraction of crystal, amorphous and rigid amorphous phases

	T_g (°C) (±1°C)[a,b]	ΔH_f^T (J g^{-1}) (±2 J g^{-1})[a]	ΔH_f^R (J g) (±2 J g^{-1})[a]	ΔH_f^{NR} (J g^{-1}) (±2 J g^{-1})[a]	χ_c (±0.02)	χ_a (±0.02)	χ_{rap} (±0.04)
Type A	104.^{5}	32.^{9}	86.^{5}	−53.^{5}	0.30	0.41	0.29
Type B	98.^{1}	34.^{0}	80.^{4}	−43.^{8}	0.31	0.64	0.05
Type C	105.^{6}	34.^{1}	80.^{4}	−43.^{4}	0.31	0.41	0.28

[a] First decimal place digit is not significant, but is included to show the spread. Error bar was determined from consideration of the error arising from different choices of starting and ending points in the determination of the baseline for calculation of the transition
[b] T_g determined from the inflection point in the reversing (R) heat flow curve

curves, representing reversing heat flow (R), total heat flow (T) and non-reversing heating flow (NR), respectively.

The total heat flow (T) curve shows the sum of all the thermal responses of the sample, and provides the same level of information as normal d.s.c. In the T curve for Type A (*Figure 2a*), a glass transition is observed followed by a small melting endotherm with a peak maximum at 180°C. The curve then drives slightly up away from the baseline. Finally, a major melting peak is observed afterwards with a peak maximum at 280°C. In the T curve for Type B sample (*Figure 2b*), after the glass transition, no endo- or exothermic activities are found until 210°C, the temperature to which the sample has previously been briefly exposed. After 210°C, the total heat flow (T) curve again goes up away from the baseline, and is followed by the major melting endotherm with a peak maximum at 280°C. In the T curve from Type C sample (*Figure 2c*), a smaller endothermic peak is first observed at the exact temperature where the small endothermic peak of Type A sample appears (near 180°C). Then, as the temperature increases, the same kind of features are seen in the Type C sample as are seen in the Type B sample. Judging by these total heat flow curves alone, it is hard to tell exactly what the thermal history effect is on either the amorphous phase or the crystalline phase. To separate the thermal history effect, we must compare the two other heat flow curves, R and NR, that represent different physical processes.

For the reversing heat flow (R) curve, Type A sample (*Figure 2a*) shows a broad glass transition, an endothermic step and a melting endotherm. For the Type B sample (*Figure 2b*), the endothermic step shifts to a higher temperature, while the major melting peak stays at the same temperature. The same features are observed in Type C sample (*Figure 2c*) as in Type B sample. No appreciable change in the reversing heat flow curve is observed in the re-annealed temperature region. In order to show these features more clearly, we have plotted the derivatives of the R and NR curves in *Figures 3a* and *b*, respectively. In *Figure 3a* (derivative of the R curves), the first shallow peak below 120°C is the result of the glass

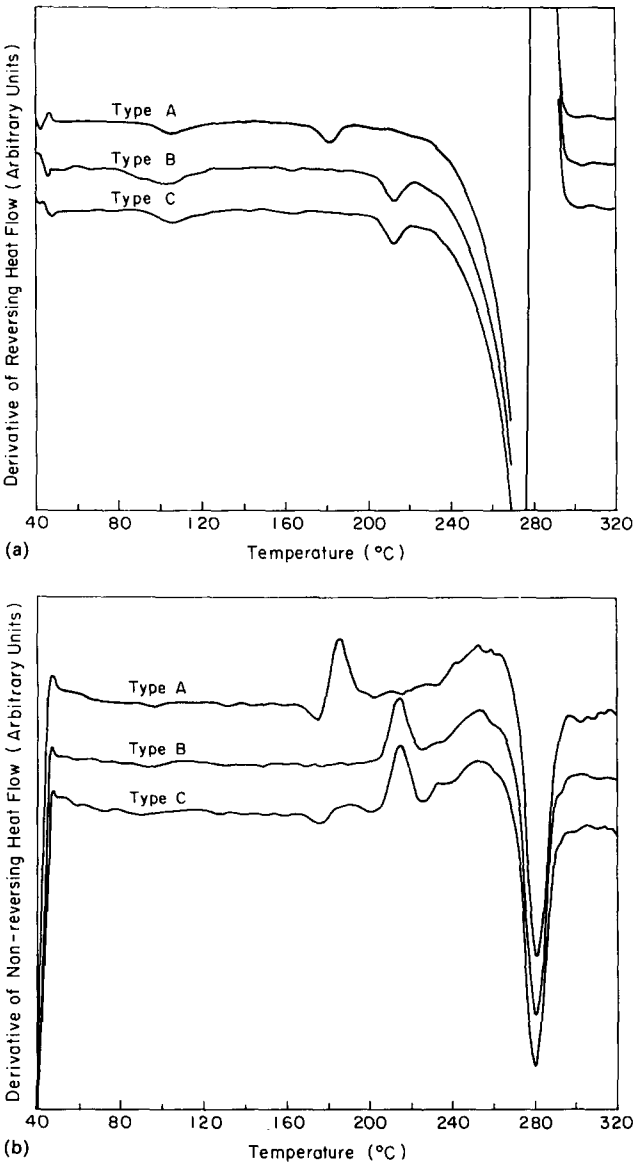

Figure 3 Derivative curves of: (a) reversing heating flow, and (b) non-reversing heat flow for three types of samples. Refer to the text for the different thermal treatments for Type A, Type B and Type C samples

transition, while the second represents the lower melting peak. The results show clearly that brief heating to the higher temperature of 210°C shifts the lower temperature peak up. Reannealing at a lower temperature of 170°C leaves no mark even on the derivatives of the R curves.

We also note in *Figure 3a* the difference among these samples at the glass transition region. After careful analysis of the R curves, we list in *Table 1* the glass transition temperature T_g (from the inflection point in the heat capacity step) and the amount of liquid-like amorphous phase, χ_a. χ_a is the ratio of the heat capacity step at $T = T_g$ of the semicrystalline sample to completely amorphous sample, and is expressed as[9–13,16]:

$$\chi_a(T) = C_p^{sc}(T)/C_p^a(T) \quad (1)$$

Type A and C show similar values of T_g and χ_a, while Type B shows a much lower T_g and larger fraction for χ_a. Thus briefly heating to a high temperature increases the amount of the liquid-like amorphous phase that is able distinctly to relax at T_g.

Also listed in *Table 1* are the crystal heats of fusion, ΔH_f^i, where the superscript i represents from which curve the value has been derived (i = T, R, or NR). ΔH_f^T has been used to calculate the initial crystallinity of the sample, χ_c, using $111.6\,J\,g^{-1}$ as the heat of fusion of 100% crystalline PPS[13]. Little difference is observed in initial crystallinity among these samples. Since the endothermic areas under the reversing heat flow (R) curves indicate the melting of already-formed crystals and those which crystallized during the scan, a decrease in ΔH_f^R from A to B (or C) reflects the fact that fewer crystals formed during the scans in samples B and C.

The amount of the rigid amorphous phase is calculated in the normal way from a three phase assumption using:

$$\chi_{rap} = 1 - \chi_c - \chi_a \quad (2)$$

A significant increase in χ_a has been found in the Type B sample over the Type A sample, resulting in a decrease in χ_{rap}. At the same time, T_g also decreases indicating a less constrained amorphous phase. However, after

reannealing, as in the Type C sample, both χ_{rap} and T_g return to values very close to those of the Type A sample.

Many features not accessible through normal d.s.c. can be observed in the NR curves. First, cold crystallization exotherms have been observed for all the samples as shown in *Figure 2*. The exothermic heat flow starts as soon as the temperature of the scan exceeds the highest temperature to which the samples had been exposed. Second, some small features can be observed in the lower temperature region, and these are shown more clearly in the derivative curves in *Figure 3b*. For the Type A sample, a downward enthalpic relaxation peak is seen around 174°C, followed first by an immediate upturn peak at 185°C, then by a broader peak at 250°C and a large downward peak at 280°C. In the Type B curve, the baseline near 160–200°C is comparatively flat; no downward peak shows up before the upturn peak that appears around 210°C. At a higher temperature, the same features have been observed in the type B sample as in the Type A sample. In the Type C curve, a downward enthalpic relaxation peak occurs at a temperature of 174°C. It is followed later by an upturn peak appearing at 214°C with a peak shape similar to that seen in the Type B sample. The same features are observed once again in the higher temperature region (above 230°C) as in the previous two curves. Reannealing at lower temperature affects the shape of the NR curve.

Discussion

For the sample initially cold crystallized at 170°C (Type A), we observe changes in both R and NR curves when the scanning temperature reaches 170°C. The step-like transition in the R curve indicates the start of melting of crystals formed at the treatment temperature, while the small downward peak from the NR curve is the result of the enthalpic relaxation of the associated amorphous phase. The step-like melting transitions have also been observed in our m.d.s.c. study of PEEK polymer[35]. The shapes of these endotherms and enthalpic relaxation peaks cannot be clearly distinguished from normal d.s.c. studies, or from the total heat flow (T) curves in m.d.s.c. since endo- and exothermic responses occur in additive contribution. Here, we suggest that the lower endotherm seen in normal d.s.c. and seen here in the R curves, results primarily from crystal melting and, to a much lesser extent, to enthalpic relaxation. One conclusion of this work is that the major contribution to the lower temperature endotherm seen near 174°C comes from crystal melting.

Amorphous phase enthalpic relaxation contributes a very minor, but nonetheless observable, component to the lower melting endotherm in the cold crystallized samples. However, this enthalpic relaxation component disappears in the Type B sample after brief heating to 210°C. At the same time as the enthalpic relaxation disappears, the amount of the rigid amorphous phase also practically disappears (dropping from 0.29 to 0.05 by weight). The liquid-like amorphous phase increases and the glass transition temperature decreases to 98°C (see *Table 1*). All these changes accompany a brief exposure of the sample to 210°C. One very plausible explanation of these events is that RAP was relaxed during the brief heating to 210°C. RAP was initially created in the Type A sample by cold crystallization at 170°C, and it became relaxed by brief heating to 210°C. We know from prior studies[13–16] that the weight fraction of RAP tends to decrease, and χ_c tends to increase, as the cold crystallization temperature increases. In addition, our dielectric relaxation studies did show that RAP relaxed little by little as the temperature was increased during the dielectric tests[9,10,14]. What our present study implies is that brief heating to a higher temperature relaxes some of the constraints on the amorphous phase, initially causing RAP nearly to disappear. If the holding time at 210°C were increased so that cold crystallization occurred, more crystals would form, and the RAP fraction would increase to the values cited in prior studies of cold crystallization[9–11,13,14].

In a very significant observation, we see that a large RAP fraction reappears in the Type C sample after reannealing at 170°C. No change in the crystal fraction was observed after this treatment. At the same time that the RAP reappears, the enthalpic relaxation peak reappears in the NR curve and the glass transition temperature increases close to its value in the Type A sample. Observation of the enthalpic relaxation peak in the Type C sample suggests that this sample has undergone a physical aging process within the amorphous phase upon holding the sample at a temperature above T_g. The process may involve changes such as densification near the crystal/amorphous interphase, which constrains more of the amorphous phase, resulting in an increase in the amount of RAP. These results are consistent with those of Struik[39,40] who studied physical aging in semicrystalline polymers. Sauerbrunn *et al.*[36] also used m.d.s.c. to study the effect of aging on the relaxation of amorphous PET. They found that enthalpic relaxation obtained from the NR curve reflected the degree of physical aging of the amorphous phase.

For the sample reannealed at 170°C (Type C), we observe no appreciable changes in either the R curve or its derivative compared to the Type B sample. This indicates that reannealing the sample at a lower temperature after exposure to higher temperature does not change the crystal phase. More importantly, we observe in the derivatives of NR curve that the enthalpic relaxation occurs at the reannealing temperature, exactly at the same place as we observe the relaxation for the Type A sample. This observation supports the view that the amorphous phase in semicrystalline polymers has been aged above its nominal T_g. Provided with the fact that annealing ages the amorphous phase and increases T_g, we suggest that annealing may be responsible for the increase of RAP in the Type C sample. The origin of RAP thus seems to be within the amorphous phase, rather than in a separately located amorphous phase as has been recently suggested for melt crystallized samples[41].

It is also worth pointing out that in all cases, reorganization was observed right above T_a as indicated by the exothermic peaks observed in the NR curves. Since cold crystallization usually results in small and imperfect crystals, once the samples have been melted at higher temperature, they tend to form more perfect crystals that are stable at a higher temperature. Quantitatively, we observe a decreased value in ΔH_f^{NR} for Type B and Type C samples. This is simply because the temperature window for reorganization becomes narrower as the cold crystallization temperature

increases. These results are direct evidence that support the theory of reorganization in the polymer cold crystallized from the quenched amorphous state.

Conclusions

1. The lower temperature endothermic peak results primarily from melting of the crystals formed at T_{cc}, and to a much lesser extent from the enthalpic relaxation of the associated amorphous phase.
2. Upon brief exposure to $T > T_{cc}$, the liquid-like amorphous phase increases, T_g decreases, RAP fraction decreases, and no enthalpic relaxation peak is observed. These results indicate that RAP (which represents a portion of the amorphous phase that is constrained) is relaxed under these conditions, and strongly suggests that the location of RAP is within the amorphous phase.
3. RAP is recreated by reannealing at T_{cc}. When the RAP fraction is restored, T_g increases and the enthalpic relaxation peak is again observed. Thus, in addition to the creation of RAP during cold crystallization, it may also be created by lower temperature annealing of the now-relaxed amorphous phase.
4. From the NR curves direct evidence has been obtained for the occurrence of crystal reorganization/recrystallization in the cold crystallized polymer[32,33]. Reorganization takes place immediately when the sample temperature reaches the previous treatment temperature.

Acknowledgements

Research is supported by the U. S. Army contract DAAH04-94-G-0317. We thank Dr Leonard Thomas and Mr David Geller from TA Instruments for providing the m.d.s.c. and for the discussions of m.d.s.c. experimental parameters.

References

1 Flory, P. J., Yoon, D. Y. and Dill, K. A. *Macromolecules* 1984, **17**, 862
2 Yoon, D. Y. and Flory, P. J. *Macromolecules* 1984, **17**, 868
3 Popli, R., Glotin, M., Mandelkern, L. and Benson, R. S. *J. Polym. Sci.* 1984, **22**, 407
4 Hahn, B., Wendorff, J. and Yoon, D. J. *Macromolecules* 1985, **18**, 718
5 Hahn, B., Herrmann-Schonherr, O. and Wendorff, J. H. *Polymer* 1987, **28**, 201
6 Lau, S. F. and Wunderlich, B. *J. Polym. Sci., Polym. Phys. Edn* 1984, **22**, 379
7 Grebowicz, J., Lau, S. F. and Wunderlich, B. *J. Polym. Sci., Polym. Symp.* 1984, **71**, 19
8 Suzuki, H., Grebowicz, J. and Wunderlich, B. *Macromol. Chem.* 1985, **186**, 1109
9 Huo, P. P. and Cebe, P. *Macromolecules* 1992, **25**, 902
10 Cebe, P. and Huo., P. P. *Thermochim. Acta* 1994, **238**, 229
11 Cheng, S. Z. D., Cao, M. Y. and Wunderlich, B. *Macromolecules* 1986, **19**, 1868
12 Jonas, A. and Legras, R. *Macromolecules* 1993, **26**,813
13 Huo, P. P. and Cebe, P. *Colloid Polym. Sci.* 1992, **270**, 840
14 Huo, P. P. and Cebe, P. *J. Polym. Sci., Polym. Phys. Edn* 1992, **30**, 239
15 Lu, S. X., Cebe, P. and Capel, M. *Macromolecules* (submitted)
16 Cheng, S. Z. D., Wu, Z. Q. and Wunderlich, B. *Macromolecules* 1987, **20**, 2802
17 Schlosser, E. and Schonhals, A. *Colloid Polym. Sci.* 1989, **267**, 963
18 Schick, C. and Nedbal, J. *Progr. Colloid Polym. Sci.* 1988, **78**, 9
19 Cebe, P. *J. Mater. Sci.* 1986, **23**, 3721
20 Chang, S. S. *Polym. Commun.* 1988, **29**, 138
21 Lee, Y. and Porter, R. S. *Macromolecules* 1987, **20**, 1336
22 Blundell, D. J. *Polymer* 1987, **28**, 2248
23 Bassett, D. C., Olley, R. H. and Raheil, I. A. M. *Polymer* 1988, **29**, 1745
24 Velikov, V., Verma, R., Prabhu, V., Dillard, D. and Marand, H. *ACS Proc. Div. Polym. Chem.* 1995, **36**, 344
25 Hsiao, B. S., Gardner, K. H., Wu, D. Q. and Chu, B. *Polymer* 1933, **34**, 3986
26 Hsiao, B. S., Gardner, K. H., Wu, D. Q. and Chu, B. *Polymer* 1993, **34**, 3996
27 Kruger, K. N. and Zackmann, H. G. *Macromolecules* 1993, **26**, 5202
28 Zhou, C. and Clough, S. B. *Polym. Eng. Sci.* 1988, **28**, 65
29 Vigier, G., Tatibouer, J., Benatmane, A. and Vassoille, R. *Colloid Polym. Sci.* 1992, **270**, 1182
30 Nichols, M. E. and Robertson, R. E. *J. Polym. Sci., Polym. Phys. Edn* 1992, **30**, 755
31 Yeh, J. T. and Runt, J. *J. Polym. Sci., Polym. Phys. Edn* 1989, **27**, 1543
32 Chung, J. S. and Cebe, P. *Polymer* 1992, **33**, 2312
33 Chung, J. S. and Cebe, P. *Polymer* 1992, **33**, 2325
34 Reading, M. *Trends Polym. Sci.* 1993, **1**(8), 248
35 Lu, X. Ph.D. Thesis, Massachusetts Institute of Technology, 1995
36 Sauerbrunn, S. R., Blaine, R. L. and Foreman, J. A. *Proc. Twenty-second Conf. North American Therm. Analysis Soc.* Sept. 1993, 514
37 Boller, A., Jin, Y. and Wunderlich, B. *J. Thermal Anal.* 1994, **42**, 307
38 Wunderlich, B., Jin, Y. and Boller, A. *Thermochim. Acta* 1993, **238**, 277
39 Struik, L. C. E. *Polymer* 1987, **28**, 1521
40 Struik, L. C. E. *Polymer* 1987, **28**, 1534
41 Sauer, B. B. and Hsiao, B. S. *Polym. Preprints* 1995, **36**(1), 261